SSRG International Journal of Electrical and Electronics Engineering
ISSN: 2348-8379/ https://doi.org/10.14445/23488379/IJEEE-V11I10P118

Volume 11 Issue 10, 174-185, October 2024

Original Article

Performance Enhancement of 3-ph 4-Switch Shunt Active Power Filter with Fuzzy-Based Control for Grid Connected Application

B. Pranith Kumar[1], K. Ravi Kumar[2], E. Vidyasagar[3]

[1]*Department of Electrical Engineering, Osmania University, Hyderabad, Telangana, India.*
[2]*Department of Electrical and Electronics Engineering, Vasavi College of Engineering, Hyderabad, Telangana, India.*
[3]*Department of Electrical Engineering, Osmania University, Hyderabad, Telangana, India.*

[1]*Corresponding Author : pranithkumar.235@gmail.com*

Received: 12 August 2024 Revised: 11 September 2024 Accepted: 12 October 2024 Published: 30 October 2024

Abstract *- Increased power demand for EVs in the present day, which may increase in the future, causes more harmonic changes in the grid. Electric vehicles need DC voltage to charge the battery packs, so AC-DC converters are used with higher current ratings. The harmonic content in the grid voltages and currents is elevated due to the increased non-linear power demand. In conventional methods, the 3-ph SAPF filters the harmonics generated by non-linear loads. The conventional 3-ph SAPF has six switches connected to a grid controlled by a synchronization controller. In this paper, the conventional six-switch SAPF is replaced with a 4-switch SAPF, reducing the switching losses and cost of the module. For the analysis, the traditional grid is upgraded to the smart grid with renewable DG units and an EV charging station, which introduces more disturbances in the grid. In order to improve the performance of the 4-switch SAPF for the smart grid, the controller is integrated with the FLC module. The FLC tends to stabilize the SAPF module, further reducing the harmonics in the grid voltages and currents. A comparative analysis is carried out between the 4-switch SAPF and the proposed FLC-based SAPF to determine the better module. The validation of a better controller module is determined by comparing the harmonic reduction capability of the SAPFs. The analysis is carried out in the MATLAB Simulink environment utilizing the library's 'Powersystem' block sets.*

Keywords *- Shunt Active Power Filter (SAPF), Distribution Generation (DG), Electric Vehicle (EV), Fuzzy Logic Controller (FLC), Matrix Laboratory (MATLAB).*

1. Introduction

With rising climatic disasters due to global warming, it is high time to shift electrical power generation to renewable sources. Fossil fuel power generation using coal or diesel contributes about 40% of environmental pollution. The remaining pollution of 50-60% is caused by the Internal Combustion (IC) engine vehicles used for either commercial or domestic transportation purposes. Commercial vehicles like public transportation (buses, medium locomotives) have a very low share, causing pollution. Domestic vehicles (cars, bikes, small locomotives) have a greater share in the global pollution index in the range of 40%. These domestic vehicles need to be replaced by EVs that run on electrical storage power and drive an electrical motor.

The power to the battery packs (for charging) needs to be provided by the renewable DG unit with a grid interface [1]. The grid provides deficit power during higher load power demand conditions, keeping the system stable. Therefore, the renewable DG unit must be synchronized with the grid voltages to transfer the power to the loads. As most renewable sources are unpredictable, power electronic circuit topologies are utilized to stabilize the DG unit. Along with the renewable DG unit power circuits, the EV charging station includes high-rating power circuits to charge the high-capacity EV battery packs [2]. Due to the many switching devices interconnecting to the grid, the health of the grid voltages and currents will drop. The EV charging station is considered to have a heavy non-linear load as the module includes high-rating AC-DC converters. The renewable DG unit also includes high-rating DC-AC inverters for synchronized power sharing. These devices create huge harmonics in the grid voltages and currents, which may impact the other loads and sources connected to the same grid.

In order to address this issue and mitigate the harmonic content in the grid voltage and currents, a transformerless SAPF is introduced at the Point of Common Coupling (PCC), where all the modules are connected at a point [3]. The conventional SAPF includes six switches forming three legs

connected to the grid through an impedance filter. SAPFs require complex control algorithms to identify and mitigate harmonics in real time effectively. Designing and implementing these algorithms can be challenging, particularly in systems with high switching frequencies or complex loads. The power electronic switches used in SAPFs contribute to energy losses, especially at higher switching frequencies, which reduces the system's overall efficiency. Additionally, the performance of SAPFs is significantly influenced by system conditions such as voltage fluctuations, load variations, and network impedance. These factors can sometimes compromise their effectiveness in improving power quality.

The conventional six-switch SAPF has higher switching losses and increased cost, which creates a limitation for small grid systems. To solve this increased power loss, the six switch SAPF is replaced with four switch SAPF. The reduced switch count decreases the switching losses and the module's cost. As the number of switches is reduced, the volumetric size and heat generation are also reduced. This proposed four switch SAPF topology is connected to the smart grid with a renewable DG unit and EV charging station to mitigate harmonics in the voltages and currents of the grid [4]. The schematic outline of the proposed smart grid system with all the mentioned modules can be observed in Figure 1.

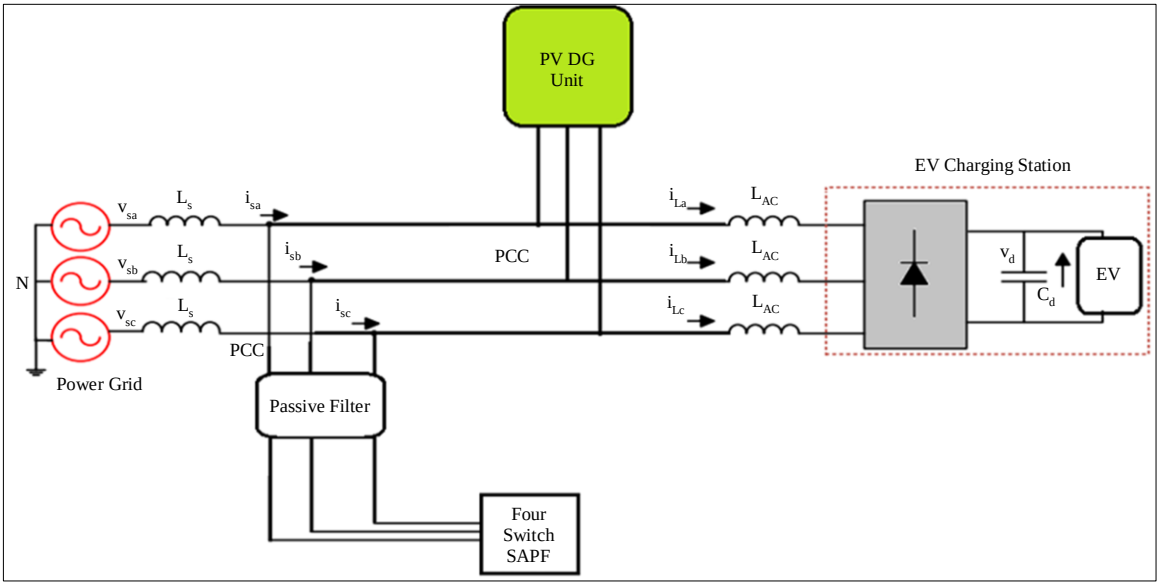

Fig. 1 Schematic of the proposed system with four switch SAPF smart grid

As per the schematic diagram, the renewable DG unit considered is a Photovoltaic (PV) plant that generates power using natural solar irradiation [5]. The power from the PV DG unit is shared with the grid through a two-stage converter module (DC-DC converter and DC-AC inverter). The EV charging station is considered a non-linear load connected with a rectifier and a DC-DC converter to control the charging power of the EV battery pack. The four switch SAPF includes four IGBT switches (S1-S4) connected to a DC link capacitor on the DC side [6].

The SAPF is connected to the grid at PCC through a passive filter (LC) to mitigate harmonics generated by the SAPF. To improve the performance of the four switch SAPF, the module controller is updated with an FLC controller, replacing the traditional PI controller [7]. The PI controller has a higher gain response, which creates disturbances in the reference signals, reducing harmonic compensation. When the PI is replaced with FLC, the disturbances in the signals are reduced, and better harmonic compensation can be achieved.

This paper is organized with an introduction in Section 1, which includes the proposed system and the modules connected to it. Section 2 has the configuration of the PV DG unit and the proposed SAPF design. Section 3 includes the control structure design for the SAPF and the modeling of FLC. The results of the proposed controllers (PI and FLC) are analyzed and compared in Section 4, validating the better control module for the system. Section 5 is the conclusion of the paper, which determines the best system and discusses the limitations of future enchantments.

2. System Configuration

The materials SAPFs are Flexible AC Transmission (FACT) devices connected to a power system grid for harmonics compensation. These devices are connected parallel to the grid between loads and the sources. These devices are connected to the grids where multiple power electronic circuits are integrated. These power electronics circuits can be either sources or loads, which are configured as per the requirement of the grid.

The harmonics intensity increases as per the grid's injected power and load power demand. The SAPF has to be configured with advanced controllers to mitigate these harmonics generated by the renewable source and non-linear load [8]. In order to achieve this, the SAPF has to be connected at PCC, where all the modules are connected at one point, filtering the harmonics generated by the modules. The placement of the SAPF restricts the harmonics from entering the grid and protects other devices connected to the grid exposed to this highly intense harmonic content. A simple grid system is considered with a 3-ph grid source, PV DG unit, EV charging station and four switch SAPF all connected at one point. The circuit configuration of the proposed smart grid with SAPF is given in Figure 2.

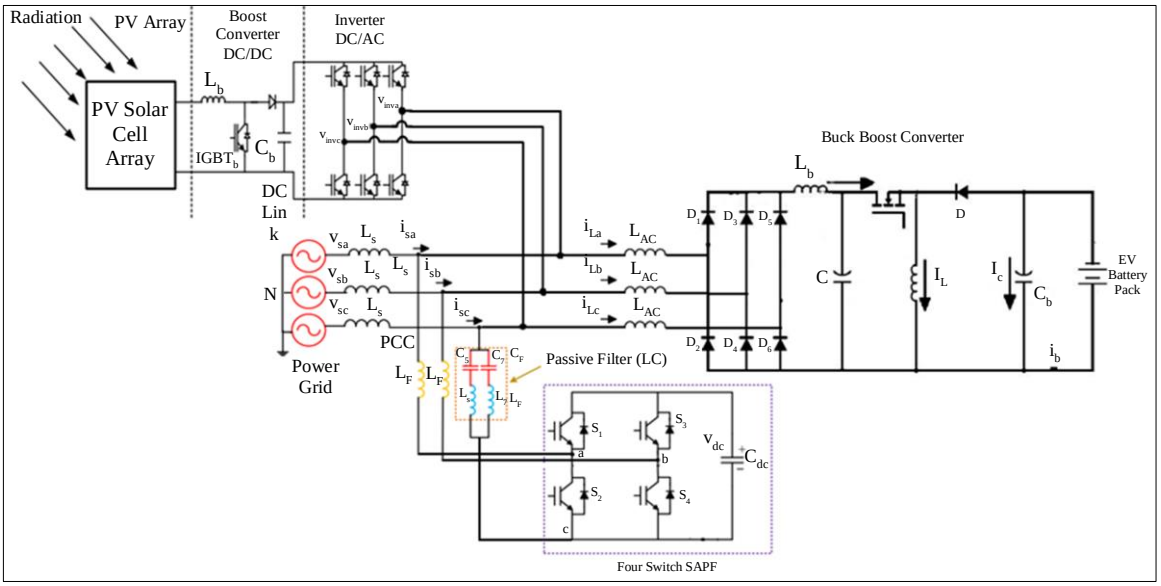

Fig. 2 Circuit configuration of the proposed system

2.1. PV Plant Configuration

As per Figure 2, the 3-ph grid source is connected to the EV charging station, PV plant and SAPF at PCC. The PV plant comprises a PV array (arrangement of parallel and series PV panels) connected to a boost converter and DC-AC inverter for voltage stability and AC voltage generation, respectively.

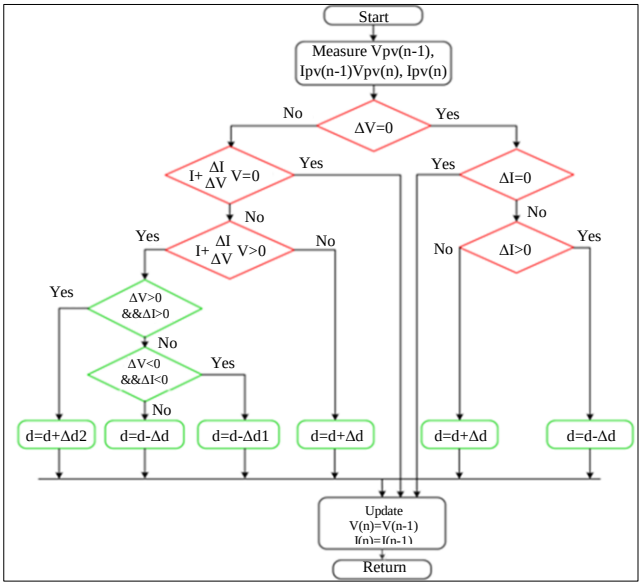

Fig. 3 Modified INC MPPT

The boost converter of the PV plant is controlled by the Maximum Power Point Technique (MPPT) with feedback from PV array voltage and current (V and I) [9].

The duty ratio (d) of the boost switch ($IGBT_b$) is changed per the solar irradiation reaching the panel. With the change in solar irradiation, there will be a change in V and I concerning which the 'd' value is updated. The flow chart of the modified Incremental Conductance (INC) MPPT can be observed in Figure 3.

As per Figure 3, it is observed that the 'd' is either increased or decreased by small variables (Δd, Δd1, Δd2). In the conventional INC MPPT, there is only one variable (Δd), which results in a lower resolution of the 'd' [10]. With three duty ratios changing variables, the modified INC MPPT has better resolution, which stabilizes the converters faster for solar irradiation changes.

The expressions for the update of 'd' are given as,

$$d = d + \Delta d \begin{cases} If\ \Delta V = 0;\ \Delta I < 0 \\ If\ \Delta V \neq 0; I + \frac{\Delta I}{\Delta V} V < 0 \end{cases} \quad (1)$$

$$d = d - \Delta d \begin{cases} If\ \Delta V = 0;\ \Delta I > 0 \\ If\ \Delta V \neq 0; I + \frac{\Delta I}{\Delta V} V > 0;\ \Delta V > 0\ AND\ \Delta I < 0 \end{cases} \quad (2)$$

$$d = d - \Delta d1 \begin{cases} If\ \Delta V = 0;\ \Delta I > 0 \\ If\ \Delta V \neq 0; I + \frac{\Delta I}{\Delta V} V > 0;\ \Delta V < 0\ AND\ \Delta I < 0 \end{cases} \quad (3)$$

$$d = d + \Delta d2 \begin{cases} If\ \Delta V = 0;\ \Delta I > 0 \\ If\ \Delta V \neq 0; I + \frac{\Delta I}{\Delta V} V > 0;\ \Delta V > 0\ AND\ \Delta I > 0 \end{cases} \quad (4)$$

As compared to Δd the $\Delta d1, \Delta d2$ have lesser value to maintain the versatility of the MPPT algorithm. As per the change in voltage and current (ΔV and ΔI) the value of 'd' is updated, and accordingly, the $IGBT_b$ is controlled for maximum power extraction from the PV array [10]. After the boost converter converts the stabilized DC voltage to 3-ph AC to share power with the grid, an SRF controller is adopted for synchronized power sharing. The SRF controller takes feedback from the grid voltages (VS_{abc}) and inverter current ($Iinv_{abc}$) for generating pulses for the DC-AC inverter.

2.2. EV Charging Station

The EV charging station combines an AC-DC converter and a DC-DC converter to limit the charging to an EV battery. The AC-DC converter is a simple Diode Bridge Rectifier (DBR) with six diodes (D1-D6), converting the 3ph AC to uncontrolled rippled DC voltage. This rippled DC voltage is stabilized and constrained to a specific voltage value by the Buck-Boost Converter (BBC) [11]. The BBC for the EV charging station is utilized for higher and lower DC voltage applications. Higher voltage levels charge four-wheeler EVs, and low voltage levels are used for two- or three-wheeler EVs. To achieve boosting voltage (Vo > Vin), the BBC switch Q1 is operated with a duty ratio above 50%, and for bucking voltage (Vo < Vin), the Q1 is operated below 50% duty ratio. A current-based control is adopted to control the charging current of the EV battery, which controls the duty ratio of Q1. The current-based control of the EV charging station is presented in Figure 4.

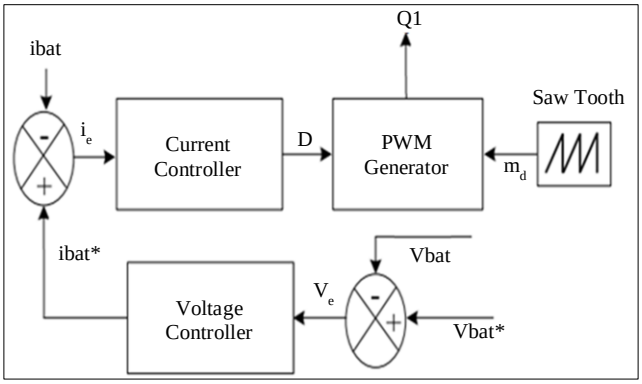

Fig. 4 Current-based control for EV charging station

As observed in Figure 4, initially, the measured EV battery voltage Vbat is compared to reference value Vbat* (set as per the battery rating) and the error signal V_e is given to the voltage controller. The voltage controller is a simple PI controller with specific proportional and integral gains generating reference current signal ibat*.

This ibat* is compared to measured battery current ibat generating error current i_e. The i_e signal is given to the current controller (PI), which generates the duty ratio (D) for the Q1 switch [12]. The D signal (between 0 and 1) is compared to a high frequency sawtooth waveform generating a pulse for Q1. As a result, the current fed to the EV battery is controlled by the ibat* value, which varies depending on the battery's state of charge.

2.3. Four Switch SAPF

The four switches SAPF is the circuit with four IGBT switches and a DC link capacitor (C_{dc}) connected in a two-legged format. The four IGBT switches form two legs, with two switches in each leg connected to two phases each. The third phase is connected at the negative terminal of the C_{dc}. To eliminate the unbalanced charging of the C_{dc}, the third phase is connected to the negative terminal of the capacitor.

The Cdc stores the power and provides ripple-reduced signals for balanced output voltages and current. Along with the SAPF a passive filter (LC) with different combinations of values is connected in series for better mitigation of harmonics [13]. This proposed four switch SAPF has enhanced capability to filter harmonics to a greater extent and create smooth voltages and currents.

The filter inductances (Lf) connected in series overcome the problem of fixed reactive power injection, which is generally present in six switch topologies. The third phase line is connected with a series combination of LC filter elements comprising specific 5^{th} and 7^{th} harmonic filtration capabilities.

Due to the connection of the third phase to the C_{dc} negative terminal the output voltage of the SAPF divides the DC voltage of C_{dc}. Due to this, the series LC filter is connected in the third phase to eliminate the unbalanced voltage and power levels on the grid side [14].

These passive filters also help to eliminate any switching ripple caused by the SAPF. The C in the LC filter generates reactive power, which is injected into the grid or load. For analyzing the four switch SAPF, an equivalent diagram is considered considering only the grid source, SAPF and load presented in Figure 5.

As per the equivalent diagram Figure 5, the grid voltages are considered Vxf (x=a,b,c), the same for load voltages as they are connected in parallel [14]. I_{sxFf} is the fundamental filtered source current, V_{invxf} and I_{cxFf} are the fundamental

voltage and compensation current of the SAPF, Z_{shf} is the impedance of the passive LC filter, and I_{Lxf} is the fundamental load current. The inverter voltage is expressed as:

$$V_{invxf} = V_{xf} - Z_{shf}.I_{cxFf} \quad (5)$$

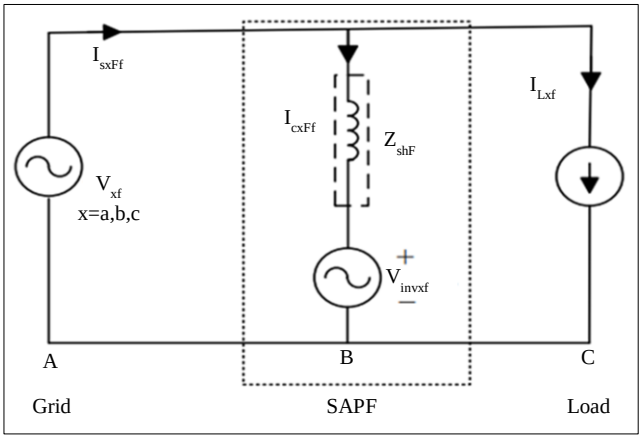

Fig. 5 Four switch SAPF equivalent circuit

The fundamental SAPF complementation current comprises active and reactive components, which are expressed as:

$$I_{cxFf} = I_{cxFfp} + I_{cxFfq} \quad (6)$$

The active power current component (I_{cxFfp}) controls the DC link voltage of C_{dc} and compensates for the losses. The reactive current component I_{cxFfq} injects reactive power into the system. The two active and reactive voltage components are expressed as:

$$V_{inv-sxfp} = V_x + I_{cxFfq}.X_{Ff} \quad (7)$$

$$V_{inv-sxfq} = -I_{cxFfp}.X_{Ff} \quad (8)$$

Here, X_{Ff} is the fundamental reactance of the LC filter. Therefore, with respect to the charge current of C_{dc}, the active and reactive current components vary. This is achieved by DC link voltage control with a specific reference voltage value set by the user as per the system's rating. The controller for the SAPF is discussed in the next section, including the FLC design.

3. SAPF Controller Design

The four switch SAPF has to be controlled as per the harmonics generated in synchronization with the grid voltages. Unsynchronized operation of the SAPF may lead to more disruptions in the grid, creating intense harmonics in the voltages and currents. This phenomenon damages the devices connected to the grid system, collapsing all the modules.

The synchronization of the SAPF is achieved by Phase Locked Loop (PLL) operating as per the grid source voltages (VS_{abc}) [6]. The complete control structure of the four switch SAPF is represented in Figure 6.

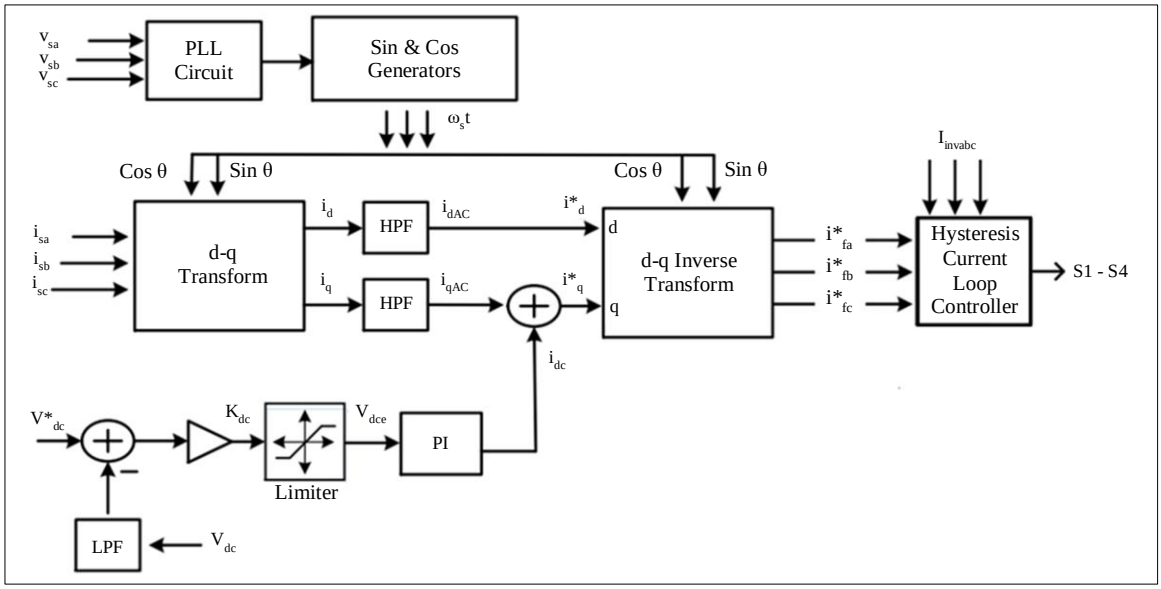

Fig. 6 Control structure of four switch SAPF

As observed in Figure 6, the reference d-q current components (i_d^*, i_q^*) are required to control the four IGBTs of the SAPF [13]. These reference d-q components are generated with respect to grid source current (iS_{abc}) harmonic content. The i_d^*, i_q^* dq-axis current components are generated by passing the measured source current dq-axis components (i_d i_q) through a High Pass Filter (HPF).

The current dq components are generated as per Park's transformation equations below.

$$i_d = V_{Sa} . Sin\,(w_s t) - V_{Sb} . Cos\,(w_s t) \quad (9)$$

$$i_q = V_{Sa} . Cos\,(w_s t) + V_{Sb} . Sin\,(w_s t) \quad (10)$$

The HPF is set with a threshold frequency of a fundamental value of 50Hz, which passes all the signals above the set value. The filtered q-axis current component (i_{qAC}) is added with the DC current component (i_{dc}) for the generation of i_q^* expressed as:

$$i_q^* = i_{qAC} + i_{dc} \quad (11)$$

The i_{dc} is generated by the PI controller with input from the comparison of reference DC voltage (v_{dc}^*) and measured DC link voltage (v_{dc}) which is expressed as:

$$i_{dc} = \frac{(v_{dc}^* - v_{dc})}{K_{dc}} \left(K_p + \int \frac{K_i}{s}\right) \quad (12)$$

The K_{dc} is the DC voltage gain for converting SI to perunit value, K_p and K_i are the proportional and integral gains of the DC voltage PI regulator [14]. The final reference signals (I_{fabc}^*) for the Hysteresis current loop controller are generated by inverse Park's transformation expressions given as:

$$I_{fa}^* = i_d^* . Sin\,(w_s t) + i_q^* . Cos\,(w_s t)$$

$$I_{fb}^* = i_d^* . Sin\left(w_s t - \frac{2\pi}{3}\right) + i_q^* . Cos\left(w_s t - \frac{2\pi}{3}\right)$$

$$I_{fc}^* = i_d^* . Sin\left(w_s t + \frac{2\pi}{3}\right) + i_q^* . Cos\left(w_s t + \frac{2\pi}{3}\right) \quad (13)$$

The pulses to the switches (S1-S4) are generated by comparing the I_{fabc}^* signals and inverter currents (I_{invabc}) fed to the hysteresis band limiter. For further updates to the SAPF control structure, the DC voltage PI regulator is replaced with FLC, improving the system's performance [15].

The FLC update reduces disturbances in the i_{dc} signal, further mitigating the harmonics in the source currents. The FLC is modeled with two input variables (E and CE) and one output variable (i_{dc}). The FLC is modeled with seven 'mamdani' type Gauss and triangular membership functions in each variable, as shown in Figure 7.

Gaussian-shaped membership functions are widely used in fuzzy logic systems, making them particularly effective for handling uncertainty and imprecision in data that follows a smooth, continuous distribution. These functions feature smooth bell-shaped curves, allowing gradual transitions between membership levels. This characteristic makes them particularly useful in applications that require soft decision boundaries. Gauss-type fuzzy systems are especially well-suited for managing uncertain or continuous input data, making them ideal for decision-making processes involving Gaussian-like distributions.

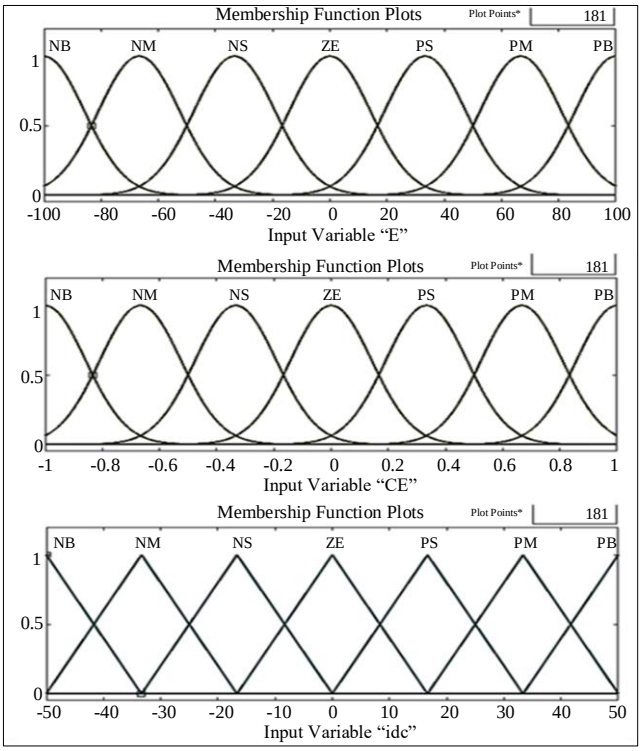

Fig. 7 FLC variables membership functions

On the other hand, triangular membership functions are straightforward, computationally efficient, and easy to interpret. These functions are triangular, resulting in a linear increase and decrease with a peak at a specific value. They are popular in applications where simplicity and quick computation are prioritized over the smoothness of transitions between membership levels. The ranges are set per the input variable value maximum upper and lower limits [16]. With a specific rule table using the IF-AND-THEN relation, the output value (idc) is generated. The fuzzy rules are given in Table 1.

Table 1. Fuzzy rules

Fuzzy Rule Table		Error (E)						
		NB	**NM**	**NS**	**ZE**	**PS**	**PM**	**PB**
Change in Error (CE)	**PB**	Z	PS	PM	PB	PB	PB	PB
	PM	NS	Z	PS	PM	PB	PB	PB
	PS	NB	NS	Z	PS	PM	PB	PB
	ZE	NB	NM	NS	Z	PS	PM	PB
	NS	NB	NB	NM	NS	Z	PS	PM
	NM	NB	NB	NB	NM	NS	Z	PS
	NB	NB	NB	NB	NB	NM	NS	Z

With the update of the DC voltage regulator in the control structure, the performance of the SAPF is analyzed using simulation modeling. A comparative analysis is done on the proposed system with both controller modules integrated into SAPF in the next section.

4. Results and Discussion

To analyze different parameters of the devices connected in the system, simulation modeling is done using the 'Powersystem' block sets of the Simulink library browser in MATLAB software. As mentioned previously in Section 2, the system is included with a 3-ph grid source, PV plant, EV charging station and four switch SAPF. The blocks of the modules are updated with the given values as per Table 2 configuration parameters. With the parameters, the system is updated, and the simulation is run with a solar plant and EV charging station. The system is then updated with four SAPF switches connected to the PCC, and the results are observed. Below are the graphs plotted for the modules' voltages, currents and powers when the simulation is run for 1sec.

Figure 8 represents the source and load 3-ph voltages and currents when the proposed system operated without SAPF. As observed, the harmonics in the source currents are very high as the system operates with all power circuit modules connected to the grid source. The switching of the circuits creates these harmonics, which need to be filtered by another device.

Table 2. Configuration parameters

Name of the Module	Parameters
3-ph Grid Source	230Vrms 50Hz, Ls =0.21mH, Lac = 3mH
PV Module	Manufacturer: SunPower SPR-305E-WHT-D Vmp = 54.7V, Voc = 64.2V, Imp = 5.58A, Isc = 5.96A, Np = 7, Ns = 5, Ppv = 10.6kW Lb = 5mH, Cin = 100µF, Co = 12mF, Δd = 0.05, Δd1 = -0.02 Δd2 = 0.02
EV Charging Station	Lf = 1.57mH, Cf = 330nF, Li = 2.5mH, C1 = 0.66µF, Lo = 4.3mH, Cd = 3200µF Rmosfet = 0.1Ω, Kp = 0.0015, Ki = 0.2, fs = 20kHz.
Four Switch SAPF	Lf = L5 = 1.9mH, L7 = 1mH, C5 = C7 = 200µF, Cdc = 4700µF, Kp = 2 Ki = 31, Fo = 50Hz, Ts = 1µsec, H = ±0.01

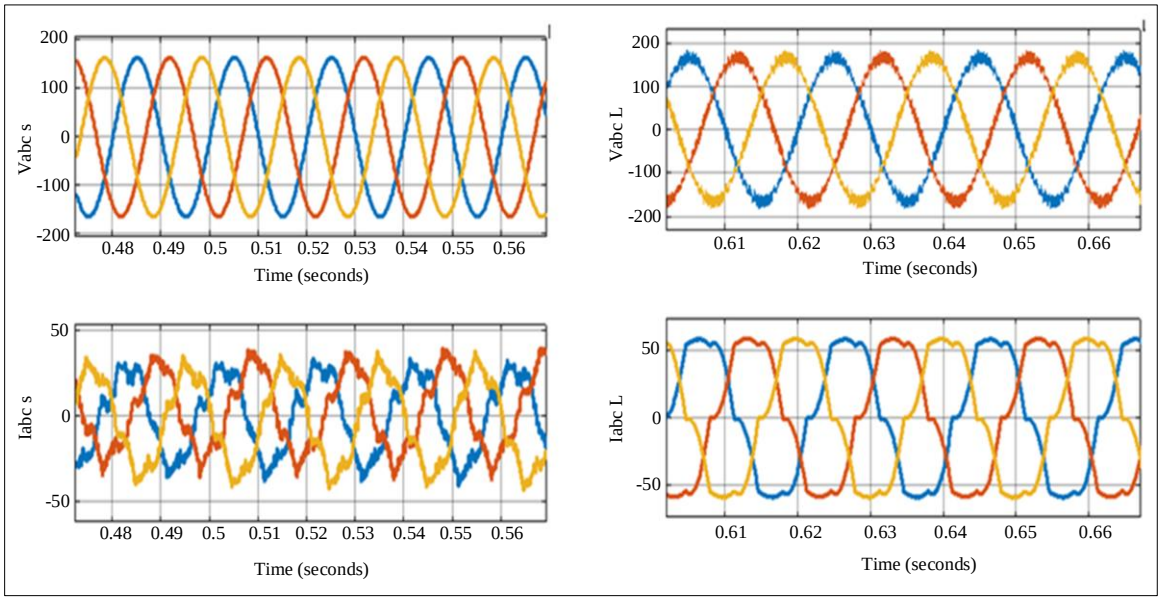

Fig. 8 Source and load voltages, currents without SAPF

Figure 9 shows the PV characteristics, which include PV voltage, current, and power, which are noted at 200V, 41A, and 8.2kW. From the total PV power of 7.8kW, the inverter injects 8kW to the grid with only 400W conversion loss. As the inverter module is connected to the LC filter, the capacitance filter injects 14kVAR into the grid for reactive power compensation. Figure 10 plots EV battery characteristics, including State of Charge (SOC), battery current and battery voltage.

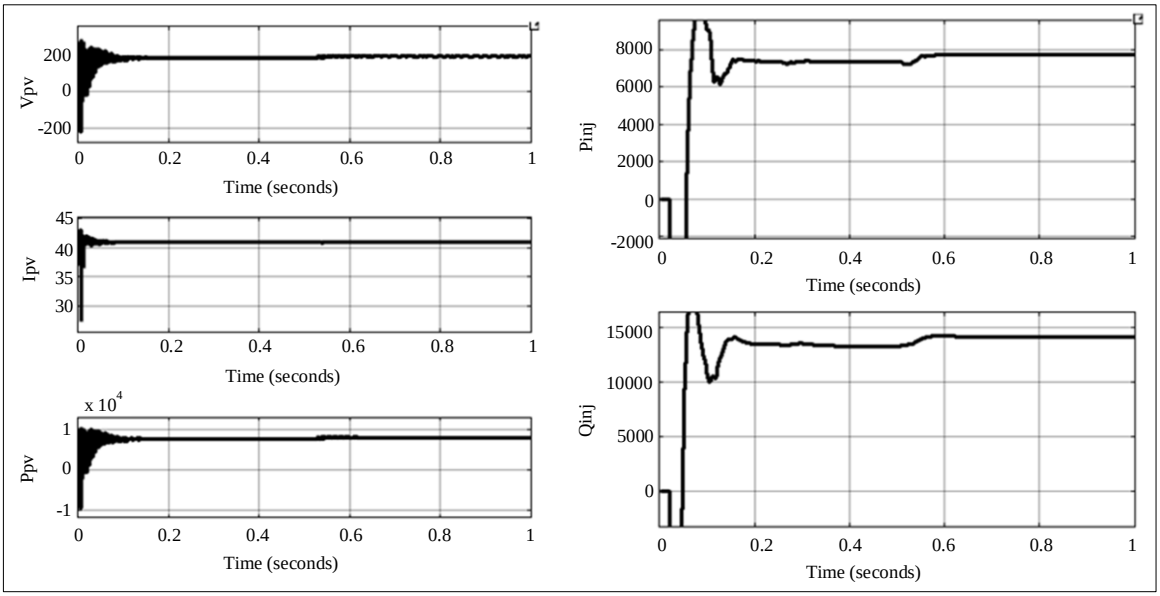

Fig. 9 PV characteristics and injected active, reactive power

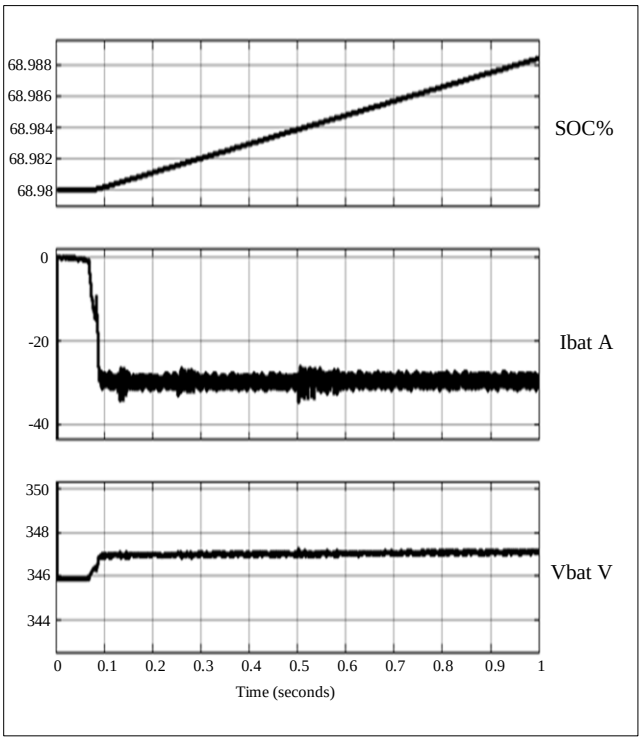

Fig. 10 EV battery pack characteristics

The rising SOC depicts that the EV battery is charging, and also, in Simulink software, the negative current of -30A represents the charging current of the battery pack. The battery voltage is set at 347V, which is the voltage when the EV battery is at 69% SOC. Figure 11 graphs the source and load 3-ph voltages and currents when the system is integrated with four switch SAPF at PCC.

It is observed that the harmonic content in the source current is drastically reduced when the SAPF is connected at the PCC. The SAPF filters the harmonics generated by the PV plant and EV charging station at the PCC and ensures near sinusoidal waveforms for the source currents. Along with harmonics compensation, the SAPF also injects reactive power into the grid by charging the Cdc, which is represented in Figure 12.

As per Figure 12, the active power injection is set to zero with a small transient during the initial stage and the reactive power injection increases to 10kVAR. The Cdc voltage stabilizes to 400V, which is the reference set in the SAPF control structure of the DC voltage regulator. Figure 13 compares the Fast Fourier Transformation (FFT) analysis tool for calculating the Total Hamonic Distortion (THD) of the source current with and without SAPF connected at the PCC of the system.

The source current THD, which was previously 22.51% when there was no SAPF, is reduced to 8.14% when the system is integrated with SAPF at PCC. The SAPF compensates for the current harmonics and ensures sinusoidal waveform generation in the grid currents. The SAPF is further updated with the FLC module replacing the DC voltage PI regulator. The modeling of the FLC module and the rule base generated per the Fuzzy rules set in Table 1 are presented in Figures 14(a) and 14(b).

The FLC modeling has two inputs (E and CE) and one output (idc) connected to a ‘saturation’ block, limiting the idc value. With the update of the FLC module in the DC voltage regulator, the simulation for the system with the same rating is run, and the THD of the source current is recorded. As per

the FFT analysis of the source current with FLC, which included four switch SAPF, the harmonics are further reduced to half from 8% to 4.36%, which is observed in Figures 15(a) and 15(b), respectively. Therefore, there is a significant decrease in the harmonic content when the system is connected with a SAPF.

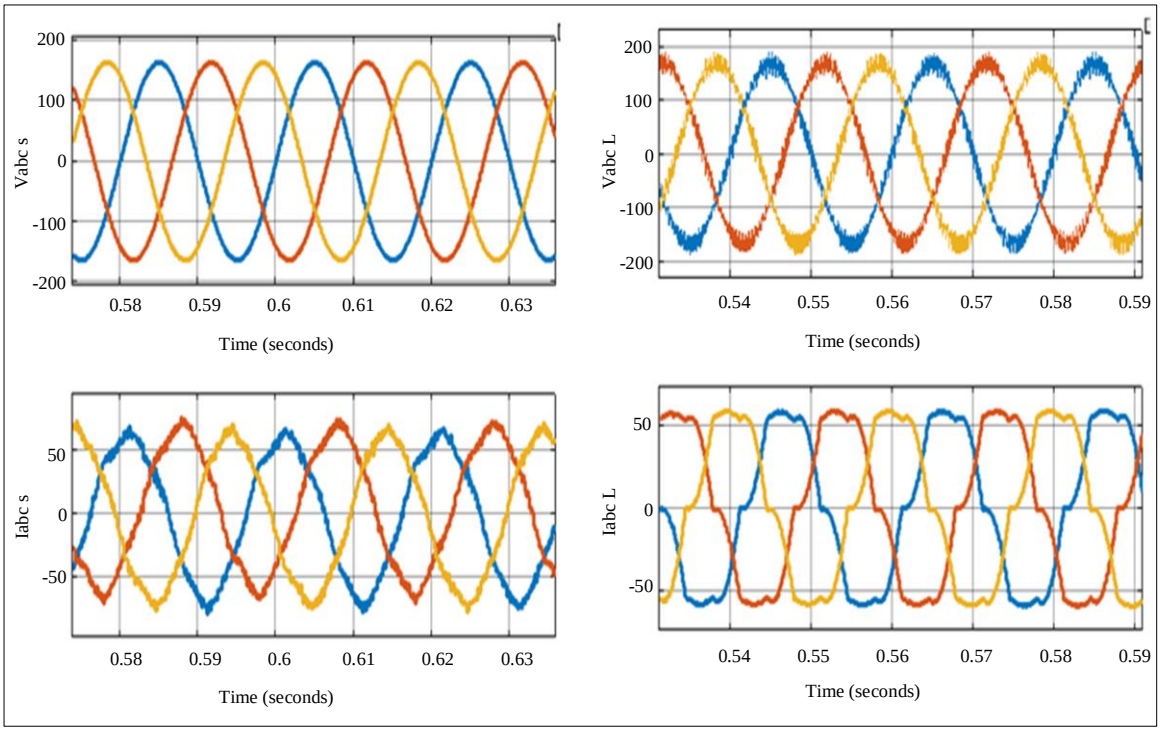

Fig. 11 Source and load voltages, currents with SAPF

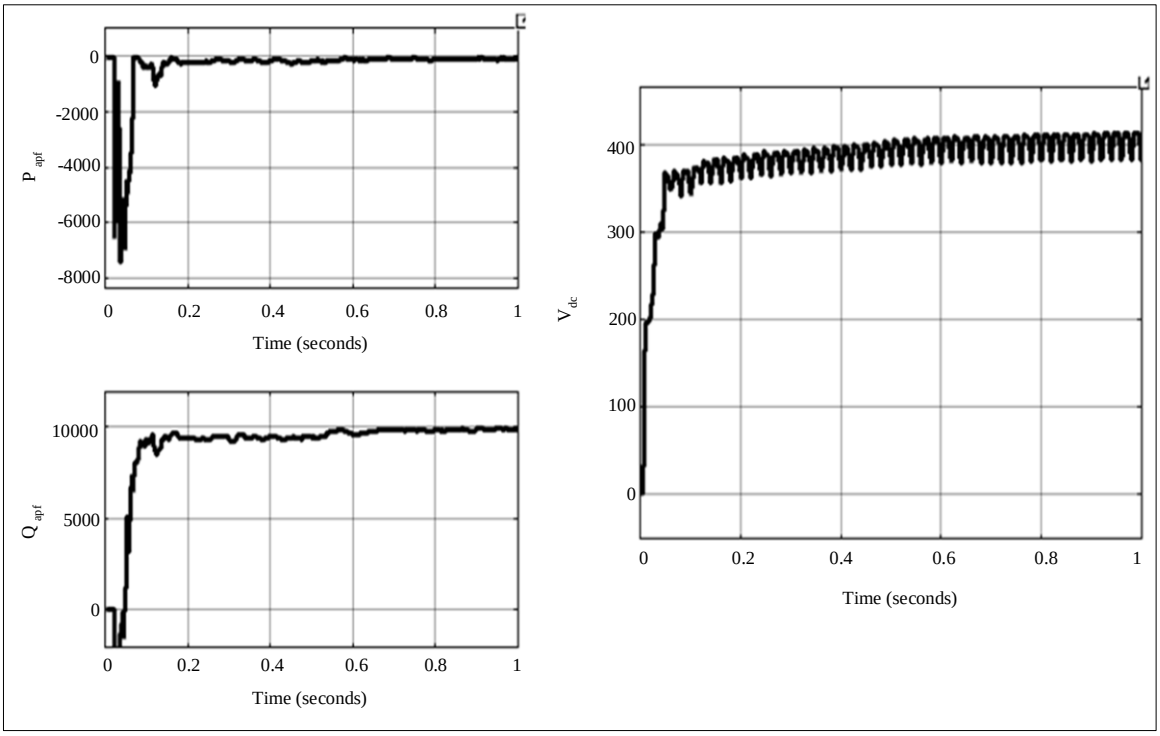

Fig. 12 SAPF active, reactive power and DC link voltage

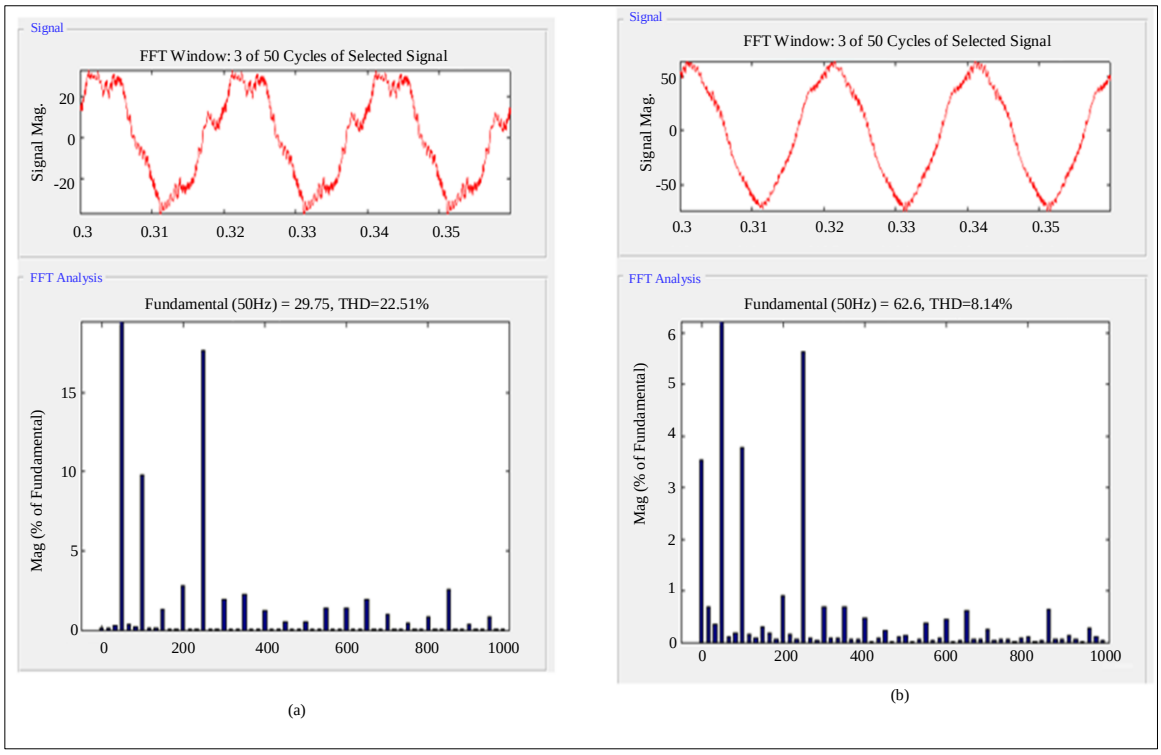

Fig. 13 THD of source current a) without SAPF, and b) with SAPF operated by PI controller.

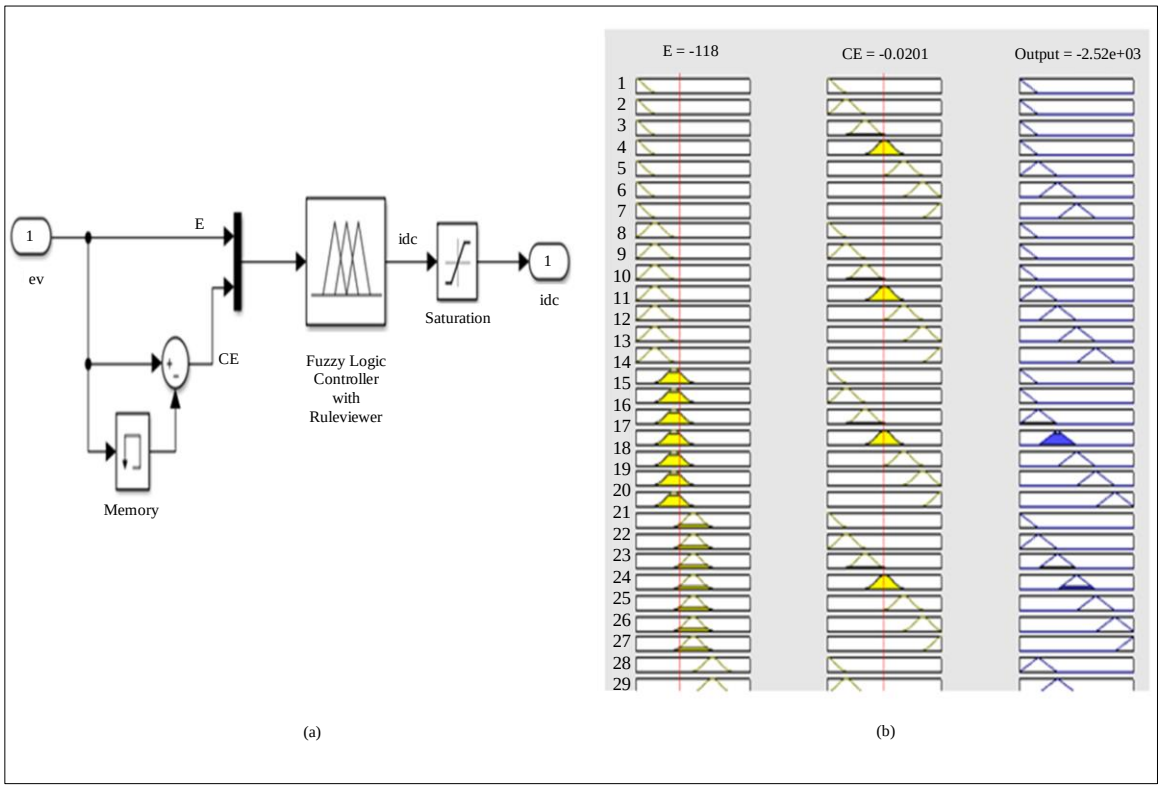

Fig. 14(a) FLC modeling, and (b) Rule viewer.

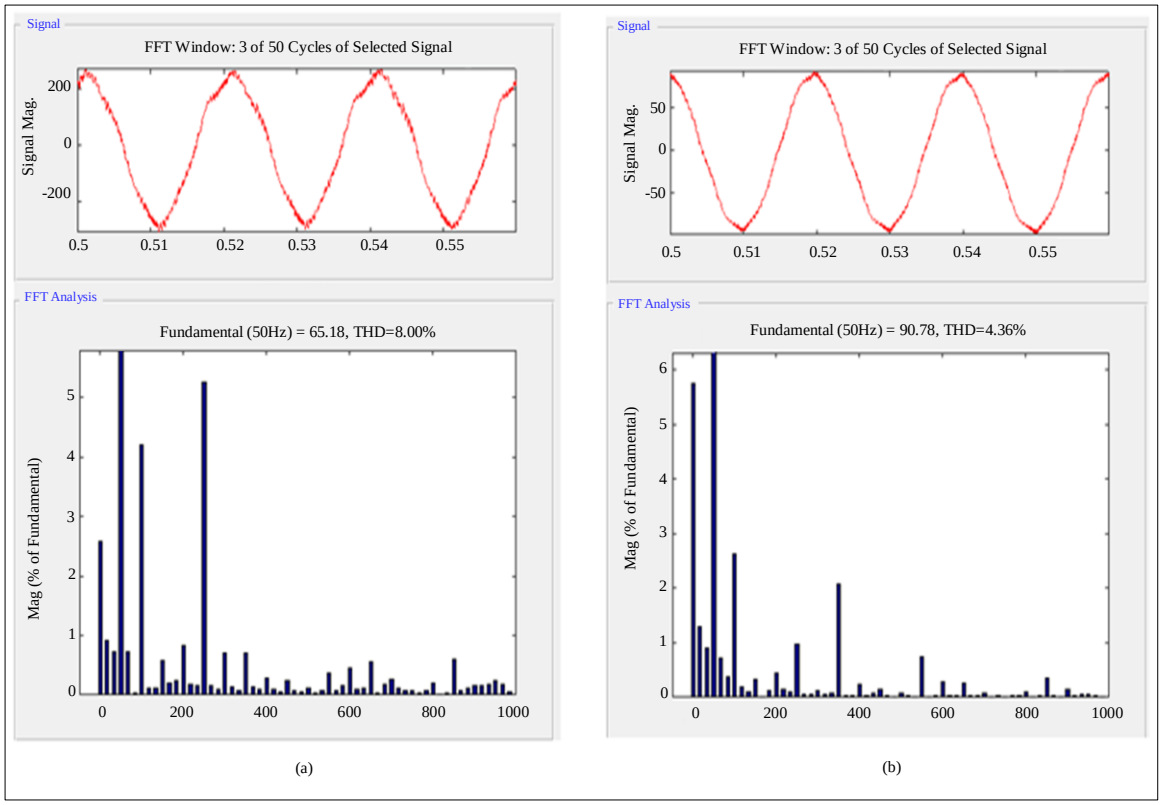

Fig. 15 THD of source current (a) with SAPF operated by PI controller, and b) with SAPF operated by FLC.

Further improvement in the performance of the SAPF is observed when the SAPF controller is updated with the FLC module. A source current THD comparison Table 3 is given below comparing the THDs with different operating conditions.

Table 3. THD comparison table

System Type	Source Current THD%
Without SAPF	22.51%
With SAPF – PI Controller	8.14%
With SAPF – FLC Module	4.36%

5. Conclusion

In this paper, a successful modeling and design of four switches SAPF are connected to a smart grid with a PV plant and EV charging station. The importance of power filters in a smart grid with multiple power electronic circuits has been addressed. With increasing non-linear load demand (EV charging) on the grid, power enhancement tools must also be updated. The drawbacks of traditional six switch SAPF have also been discussed, and the merits of the four switch SAPF are also presented. The proposed grid system with these modules is simulated without SAPF, with the SAPF – PI controller and SAPF – FLC module connected to PCC. The source currents of the grid are analyzed and compared using the FFT analysis tool present in 'powergui' of Simulink. As per the analysis, it is validated that the system operated with the SAPF – FLC module mitigates the harmonics to below 5% as per the IEEE 519-2022 standard. The THD value recorded is 4.36%, which can be further reduced to lower values by updating the SAPF controller with adaptive or hybrid controllers.

References

[1] M.S. Arjun et al., "Impact of Electric Vehicle Charging Station on Power Quality," *International Journal of Applied Power Engineering*, vol. 13, no. 1, pp. 186-193, 2024. [CrossRef] [Google Scholar] [Publisher Link]

[2] Antonio Venancio M.L. Filho et al., "Impact Analysis and Energy Quality of Photovoltaic, Electric Vehicle and BESS Lead-Carbon Recharge Station in Brazil," *Energies*, vol. 16, no. 5, 2023. [CrossRef] [Google Scholar] [Publisher Link]

[3] Priyanka Mane, and Rajin M. Linus, "Power Quality Issues in Solar Powered Fast Charging Station for Electric Vehicle: Comprehensive Review & Mitigation Measures," *2023 IEEE 8th International Conference for Convergence in Technology (I2CT)*, Lonavla, India, pp. 1-9, 2023. [CrossRef] [Google Scholar] [Publisher Link]

[4] Vandana Jain, Bhim Singh, and Seema, "A Grid Connected PV Array and Battery Energy Storage Interfaced EV Charging Station," *IEEE Transactions on Transportation Electrification*, vol. 9, no. 3, pp. 3723-3730, 2023. [CrossRef] [Google Scholar] [Publisher Link]

[5] Chi-Seng Lam et al., "Adaptive Thyristor-Controlled LC-Hybrid Active Power Filter for Reactive Power and Current Harmonics Compensation with Switching Loss Reduction," *IEEE Transactions on Power Electronics*, vol. 32, no. 10, pp. 7577-7590, 2017. [CrossRef] [Google Scholar] [Publisher Link]

[6] Wajahat Ullah Khan Tareen, and Saad Mekhielf, "Three-Phase Transformerless Shunt Active Power Filter With Reduced Switch Count for Harmonic Compensation in Grid-Connected Applications," *IEEE Transactions on Power Electronics*, vol. 33, no. 6, pp. 4868-4881, 2018. [CrossRef] [Google Scholar] [Publisher Link]

[7] Suleiman Musa et al., "Modified Synchronous Reference Frame Based Shunt Active Power Filter with Fuzzy Logic Control Pulse Width Modulation Inverter," *Energies*, vol. 10, no. 6, 2017. [CrossRef] [Google Scholar] [Publisher Link]

[8] Stefani Freitas et al., "New Topology of a Hybrid, Three-Phase, Four-Wire Shunt Active Power Filter," *Energies*, vol. 16, no. 3, 2023. [CrossRef] [Google Scholar] [Publisher Link]

[9] Ahmed Ismail M. Ali et al., "An Efficient MPPT Technique-Based Single-Stage Incremental Conductance for Integrated PV Systems Considering Flyback Central-Type PV Inverter," *Sustainability*, vol. 14, no. 19, 2022. [CrossRef] [Google Scholar] [Publisher Link]

[10] Chaoping Rao et al., "A Novel High-Gain Soft-Switching DC-DC Converter with Improved P&O MPPT for Photovoltaic Applications," *IEEE Access*, vol. 9, pp. 58790-58806, 2021. [CrossRef] [Google Scholar] [Publisher Link]

[11] Chirag P. Mehta, and Balamurugan P., "Buck-Boost Converter as Power Factor Correction Controller for Plug-in Electric Vehicles and Battery Charging Application," *2016 IEEE 6th International Conference on Power Systems (ICPS)*, New Delhi, India, pp. 1-6, 2016. [CrossRef] [Google Scholar] [Publisher Link]

[12] Morris Brenna et al., "Electric Vehicles Charging Technology Review and Optimal Size Estimation," *Journal of Electrical Engineering & Technology*, vol. 15, pp. 2539-2552, 2020. [CrossRef] [Google Scholar] [Publisher Link]

[13] Bruno Nova et al., "Computer Studies of the Operation of a Three-Phase Four Wire Shunt Active Power Filter Applied to the Industry," *Sustainable Energy for Smart Cities*, pp. 119-140, 2022. [CrossRef] [Google Scholar] [Publisher Link]

[14] Chamberlin Stéphane Azebaze Mboving, and Zbigniew Hanzelka, "Investigation on the Performance Efficiency of the Shunt Hybrid Active Power Filter," *Power Quality and Harmonics Management in Modern Power Systems*, 2024. [CrossRef] [Google Scholar] [Publisher Link]

[15] Ekhlas M. Thajeel, Mazin M. Mahdi, and Eyad I. Abbas, "Fuzzy Logic Controller Based Shunt Active Power Filter for Current Harmonic Compensation," *2020 International Conference on Computer Science and Software Engineering (CSASE)*, Duhok, Iraq, pp. 94-99, 2020. [CrossRef] [Google Scholar] [Publisher Link]

[16] Mohammed Kadem et al., "Fuzzy Logic-Based Instantaneous Power Ripple Minimization for Direct Power Control Applied in a Shunt Active Power Filter," *Electrical Engineering*, vol. 102, pp. 1327-1338, 2020. [CrossRef] [Google Scholar] [Publisher Link]